Algebraic theory of crystal vibrations: Singularities and zeros in vibrations of one- and two-dimensional lattices

F. Iachello,[1,*] B. Dietz,[2,†] M. Miski-Oglu,[2] and A. Richter[2]

[1]*Center for Theoretical Physics, Sloane Physics Laboratory, Yale University, New Haven, Connecticut 06520-8120, USA*
[2]*Institut für Kernphysik, Technische Universität Darmstadt, D-64289 Darmstadt, Germany*

A novel method for the calculation of the energy dispersion relation and density of states (DOS) in one (1D) and two (2D) dimensions is introduced and applied to linear lattices (1D) and square and hexagonal lattices (2D). The (van Hove) singularities and (Dirac) zeros of the DOS are discussed. Results for the 2D hexagonal lattice (graphenelike materials) are compared with experimental data in microwave photonic crystals.

I. INTRODUCTION

Phonon energy dispersion relations (EDR) and the density of states (DOS) are a fundamental physical property of a solid especially for determining the mechanical, thermal, and other condensed matter phenomena. Although most of the interest in the past has been in three-dimensional (3D) systems, for example diamond, with the discovery of graphene [1] interest in systems of lower dimensionality has arisen, including graphene [two dimensions (2D)] [2,3], graphene tubules [one dimension (1D)] [4], and fullerenes [zero dimensions (0D)] [5].

At the same time, the development of superconducting microwave billiards [6,7] and of photonic crystals [8,9] combined into "microwave photonic crystals" or generally of "artificial graphene" [10–20], has opened the way for simulations of crystal vibrations in systems of lower dimensionality (2D, 1D, 0D) with a finite number of units.

Calculations of the EDR and the DOS in infinite systems have been done using a variety of methods, including tight-binding force-constant models [4,21,22] and molecular dynamics methods. Here, we introduce a method, based on the algebraic theory of molecules [23], which reproduces all previously known results for the fundamental vibration $v = 1$ of crystals, and, in addition, can be extended to overtone vibrations. The method is particularly well suited for analyzing the EDR and DOS of microwave photonic crystals.

With this method, we calculate the EDR and DOS of the fundamental ($v = 1$) and overtone ($v = 2$) transverse vibrations of 1D and 2D crystals. For $v = 1$ we also rederive the EDR and DOS analytically, determining the location of (van Hove) singularities and (Dirac) zeros in transverse vibrations of 1D and 2D crystals with square and hexagonal lattices. The latter is then compared with experimental results in microwave billiards. We are then able to determine the scaling behavior of the singularities.

II. ALGEBRAIC METHOD

A. One atom

We consider a one-dimensional (1d) vibration of an atom (for convenience in the z direction), and assume that it is bound by a potential

$$V(z) = -\frac{V_0 \lambda(\lambda - 1)}{\cosh^2 \alpha z},\tag{1}$$

as shown in Fig. 1. The energy levels in this potential can be described by the simple formula [24]

$$E(v) = E_0 + A(v - \xi v^2),\tag{2}$$

where $\xi = \frac{1}{2(\lambda - 1)}$ (also written, for integer λ, as $\frac{1}{N}$) describes the anharmonicity, $A = 2V_0(\lambda - 1)$ (also written as $\hbar\omega$) the oscillator frequency, and $E_0 = -V_0(\lambda - 1)^2$ the zero-point energy. It was shown in [25] that the Pöschl-Teller potential (1) can be associated with the algebra of $g \equiv u(2)$. Its eigenstates are described by representations of $u(2) \supset so(2)$, labeled by $|N,v\rangle$ where $v = 0, 1, \ldots, \frac{N}{2}$ or $\frac{N-1}{2}$ (for $N =$ even or odd) is the vibrational quantum number, and N is the so-called vibron number which determines how many bound states are in the potential. The Hamiltonian can then be written in algebraic form as

$$H = E_0 + AC,\tag{3}$$

where E_0 is the zero-point energy, A a scale, and the operator C, called Casimir operator, has eigenvalues

$$\langle N,v|C|N,v\rangle = -4\left(v - \frac{v^2}{N}\right).\tag{4}$$

From Eq. (4), one can see that N controls the anharmonicity of the potential $\xi = \frac{1}{N}$. For $N \to \infty$, the spectrum is harmonic and has an infinite number of bound states, $v = 0, 1, \ldots, \infty$. The potential (1) is therefore well suited to describe both harmonic and anharmonic vibrations.

B. Many atoms

In the case of many atoms at location $i = 1, \ldots, n$, bound by Pöschl-Teller potentials, the algebra is $g \equiv u_1(2) \oplus u_2(2) \oplus \ldots \oplus u_i(2) \oplus \ldots \oplus u_n(2)$ [26,27]. The algebraic Hamiltonian for n uncoupled oscillators is

$$H = E_0 + \sum_{i=1}^{n} A_i C_i,\tag{5}$$

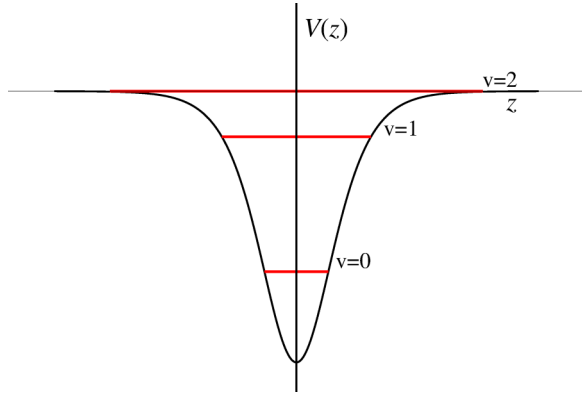*francesco.iachello@yale.edu
†dietz@ikp.tu-darmstadt.de

FIG. 1. (Color online) The Pöschl-Teller potential (1) with $\alpha = 1$, $V_0 = 1$, $\lambda = 3$.

where E_0 is the zero-point energy and A_i a scale. Its eigenvalues are

$$E = E_0 - 4 \sum_{i=1}^{n} A_i \left(v_i - \frac{v_i^2}{N_i} \right). \tag{6}$$

If all the oscillators are equivalent, $A_i \equiv A$, $N_i = N$, and

$$E = E_0 - 4A \sum_{i=1}^{n} \left(v_i - \frac{v_i^2}{N} \right). \tag{7}$$

In the harmonic limit $N_i \to \infty$, the matrix elements of the operators C_i are the familiar matrix elements of the number operator $\hat{n}_i = b_i^\dagger b_i$, where $b_i^\dagger$ (b_i) are boson creation and annihilation operators of a phonon at site i, multiplied by -4.

The phonons (vibrons) interact with a diagonal and an off-diagonal interaction. The diagonal interaction is written in terms of the normalized Casimir operator C_{ij} of the combined $so_i(2) \oplus so_j(2)$ algebra as

$$\langle N_i, v_i; N_j, v_j | C_{ij} | N_i, v_i; N_j, v_j \rangle$$
$$= -4 \left[(v_i + v_j) - \frac{(v_i + v_j)^2}{(N_i + N_j)} \right]. \tag{8}$$

In practical calculations, it is convenient to subtract from C_{ij} a contribution that can be absorbed in the Casimir operators of the individual modes i and j given in Eq. (4), thus considering an operator C_{ij}' whose matrix elements are

$$\langle N_i, v_i; N_j, v_j | C_{ij}' | N_i, v_i; N_j, v_j \rangle$$
$$= -4 \left[\frac{v_i^2}{N_i} + \frac{v_j^2}{N_j} - \frac{(v_i + v_j)^2}{(N_i + N_j)} \right]. \tag{9}$$

The Hamiltonian for n oscillators diagonally coupled is

$$H = E_0 + \sum_{i=1}^{n} A_i C_i + \sum_{i \neq j}^{n} A_{ij}' C_{ij}'. \tag{10}$$

If all oscillators are equivalent, $N_i = N$, $A_i = A$, $A_{ij}' = A'$, and the eigenvalues are

$$E = E_0 - 4A \sum_{i=1}^{n} \left(v_i - \frac{v_i^2}{N} \right)$$
$$- 4A' \sum_{i \neq j}^{n} \left[\frac{v_i^2}{N} + \frac{v_j^2}{N} - \frac{(v_i + v_j)^2}{2N} \right]. \tag{11}$$
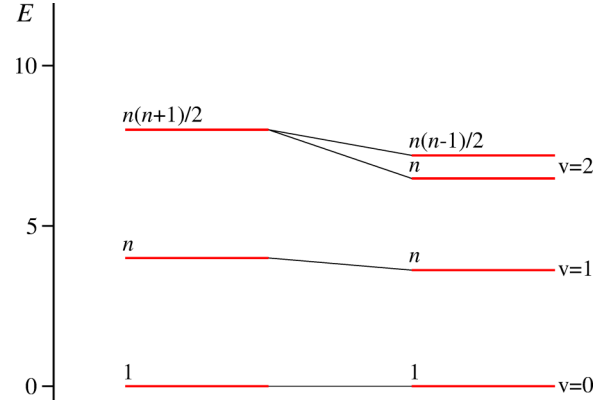

FIG. 2. (Color online) Spectrum of equivalent harmonic oscillators with diagonal interaction [Eq. (11)], with $E_0 = 0$, $A = -1$, $N = 10$, $A' = -0.1$.

The diagonal interaction represents the modification in the Pöschl-Teller potentials at each site due to the other sites. It is usually small and it can be neglected. The spectrum of states of equivalent oscillators with diagonal interaction is shown in Fig. 2 for up to two phonons $\sum_i v_i = 2$, both for harmonic ($N \to \infty$) and anharmonic oscillators. The degree of degeneracy of the levels is given in Eq. (19) and is shown to the left of the levels.

The off-diagonal interaction is written in terms of operators, called Majorana operators M_{ij}, with matrix elements [23,26,27]

$$\langle N_i, v_i + 1; N_j, v_j - 1 | M_{ij} | N_i, v_i; N_j, v_j \rangle$$
$$= -[v_j (v_i + 1)(N_i - v_i)(N_j - v_j + 1)]^{1/2} / [N_i N_j]^{1/2};$$
$$\langle N_i, v_i - 1; N_j, v_j + 1 | M_{ij} | N_i, v_i; N_j, v_j \rangle$$
$$= -[v_i (v_j + 1)(N_j - v_j)(N_i - v_i + 1)]^{1/2} / [N_i N_j]^{1/2}. \tag{12}$$

The Majorana operators have also diagonal matrix elements given by

$$\langle N_i, v_i; N_j, v_j | M_{ij} | N_i, v_i; N_j, v_j \rangle$$
$$= (v_i N_j + v_j N_i - 2 v_i v_j) / (N_i N_j)^{1/2}. \tag{13}$$

If the oscillators are equivalent, $N_i = N$, their contribution $(v_i + v_j - \frac{2 v_i v_j}{N})$ can be reabsorbed into Eq. (11) so it will not be considered further.

The operator

$$\hat{M} = \sum_{i \neq j}^{n} M_{ij} \tag{14}$$

is Hermitian and its matrix elements are real and symmetric. It is called Majorana (or exchange) operator because it was introduced by Majorana in 1933 in the context of nuclear physics [28]. Within the algebraic theory of molecules [23] it was introduced in 1991 [26]. Its mathematical definition is that of the invariant operator of $u_1(2) \oplus u_2(2) \oplus \ldots \oplus u_n(2)$. In recent years, operators similar to $\hat{M}$ have been used in the context of condensed matter physics.

The elements M_{ij} of the Majorana operator annihilate one quantum of vibration at site i and create one at site j, or vice versa. In the harmonic limit $N_i \to \infty$, the matrix elements
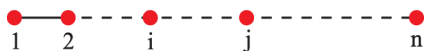
FIG. 3. (Color online) The linear lattice.

of M_{ij} are the familiar matrix elements $[v_j(v_i + 1)]^{1/2}$ of the operator $b_i^\dagger b_j$, where $b_i^\dagger$ and b_i are boson creation and annihilation operators of a phonon at site i, respectively, multiplied by a minus sign. Because of the sum in Eq. (14), $\hat{M}$ can be written as $\sum_{j>i}^n (b_i^\dagger b_j + b_j^\dagger b_i)$, which shows explicitly the Hermiticity of $\hat{M}$. The operator $\hat{M}$ splits the degeneracy of the states in Fig. 2, determines the distribution of eigenvalues and thus the level densities for the fundamental vibration $v = \sum_i v_i = 1$ and the overtones $v = 2, 3, \ldots$, and generates the normal modes of vibrations.

The total Hamiltonian for $1d$ vibrations of a system of n atoms at locations $\vec{r}_i$, $i = 1, \ldots, n$, can be written as

$$H = E_0 + \sum_{i=1}^n A_i C_i + \sum_{i \neq j}^n A'_{ij} C'_{ij} + \sum_{i \neq j}^n \lambda_{ij} M_{ij}, \quad (15)$$

and for n identical atoms as

$$H = E_0 + A \sum_{i=1}^n C_i + A' \sum_{i \neq j}^n C'_{ij} + \sum_{i \neq j}^n \lambda_{ij} M_{ij}. \quad (16)$$

This Hamiltonian applies to any system. In Secs. III, IV, and V, we will consider three cases: (1) linear lattice (1D), (2) square lattice (2D), and (3) honeycomb lattice (2D).

III. LINEAR LATTICE

The algebraic theory of linear lattices, Fig. 3, was investigated in [29]. The most general algebraic Hamiltonian for this problem can be written as

$$H = A \sum_j C_j + \lambda^{(I)} \sum_j M^{(I)}_{j,j+1} + \lambda^{(II)} \sum_j M^{(II)}_{j,j+2}$$
$$+ \lambda^{(III)} \sum_j M^{(III)}_{j,j+3} + \ldots \quad (17)$$

with $j = 1, 2, \ldots, n$, and where $\lambda^{(I)}$ is the strength of the nearest-neighbor interaction, $\lambda^{(II)}$ of the next-nearest neighbor, $\lambda^{(III)}$ of the next-to-next one, etc.

The Hamiltonian (17) is of the general form

$$H = A \sum_j C_j + \sum_{j \neq j'} \lambda_{jj'} M_{jj'}. \quad (18)$$

Denoting by $|v_j\rangle$ the number of quanta at each site j, the basis for the diagonalization of Eq. (18) is

$v = 0$	vacuum	$|0\rangle = |0,0,\ldots,0\rangle$
$v = 1$	n basis states	$|1_j\rangle = |0,0,\ldots,1_j,\ldots,0\rangle$
$v = 2$	n basis states	$|2_j\rangle = |0,0,\ldots,2_j,\ldots,0\rangle$
$v = 2$	$\frac{n(n-1)}{2}$ basis states	$|1_j,1_{j'}\rangle = |0,0,\ldots,1_j,\ldots,1_{j'},\ldots,0\rangle$
$\ldots$	$\ldots$	$\ldots$

(19)

The states with $v = 1$ constitute the fundamental vibration, the states with $v = 2$ the overtone and combination modes of the linear lattice. The matrix elements of the operators C_j are

$$\langle v_j | C_j | v_j \rangle = -4 \left(v_j - \frac{v_j^2}{N} \right) \xrightarrow{N \to \infty} -4 v_j$$

$$\langle v_j + 1, v_{j'} - 1 | M_{jj'} | v_j, v_{j'} \rangle = -\left[v_{j'}(v_j + 1)\left(1 - \frac{v_j}{N}\right)\left(1 - \frac{v_{j'} - 1}{N}\right) \right]^{1/2} \xrightarrow{N \to \infty} -[v_{j'}(v_j + 1)]^{1/2}. \quad (20)$$

In the harmonic limit $N \to \infty$, the algebraic Hamiltonian (18) reduces to the boson Hubbard Hamiltonian

$$H = -4A \sum_j b_j^\dagger b_j - \sum_{j \neq j'} \lambda_{jj'} b_j^\dagger b_{j'}, \quad (21)$$

where $b_j^\dagger$ creates a quantum at site j. For identical oscillators and nearest-neighbor interaction, it can be written as

$$H = -4A \sum_i \hat{n}_i - \lambda \sum_i (b_i^\dagger b_{i+1} + b_i b_{i+1}^\dagger), \quad (22)$$

with, in the notation of Ref. [30], $\mu = 4A$ and $t = \lambda$.

Since the operator $\sum_j C_j$ is diagonal in the basis Eq. (19) and the operator $\sum_{j \neq j'} M_{jj'}$ conserves the total number of quanta $v = \sum_j v_j$, the diagonalization of H splits into blocks. H can then be diagonalized in the subspaces with $v = 1$, $v = 2, \ldots$, of dimension $n, \frac{n(n+1)}{2}, \ldots$.

It is of interest to note that the algebraic method can also describe more complex situations such as those in which the algebraic Hamiltonian is

$$H = A \sum_i C_i + B \sum_i C_i^2 + B' \sum_{i \neq j} C_i C_j + \lambda \sum_{i \neq j} M_{ij}, \quad (23)$$

which is equivalent to the boson Hubbard Hamiltonian with in-site interactions

$$H = -\mu \sum_i \hat{n}_i + U \sum_i \hat{n}_i (\hat{n}_i - 1) + V \sum_i \hat{n}_i \hat{n}_{i+1}$$
$$- t \sum_i (b_i^\dagger b_{i+1} + b_i b_{i+1}^\dagger). \quad (24)$$

The diagonalization of this Hamiltonian can be done in the same way as before since the additional terms do not modify its block-diagonal form.

A. Solutions

1. Fundamental vibration v=1

The EDR and DOS of the fundamental vibration $v = 1$ of a linear lattice can be obtained analytically by purely algebraic methods by making use of certain properties of matrices. These properties were first noticed by Nierenberg [31] for lines and further exploited and generalized for lines and rings in Refs. [29,32]. The basic property is that the Majorana matrix on a line M_L with matrix elements

$$\langle M_L \rangle_{t,t\pm s} = c_s \tag{25}$$

on the diagonal "$\pm s$ off the main diagonal" has eigenvalues given by

$$m = c_s 2 \cos \frac{sk\pi}{(n+1)}, \quad k = 1,2,\ldots,n. \tag{26}$$

For nearest-neighbor interactions $s = 1$, the solution can be written as

$$E_k = \alpha - 2\beta \cos\theta_k, \quad \theta_k = \frac{k\pi}{(n+1)}, \quad k = 1,\ldots,n. \tag{27}$$

This solution applies to both harmonic and anharmonic vibrations. The coefficients α and β are given by

$$\alpha = -4A\left(1 - \frac{1}{N}\right), \quad \beta = \lambda. \tag{28}$$

If the number of sites is large, one can replace $\frac{k\pi}{(n+1)}$ by a continuous variable x which runs from 0 to π and E_k by a continuous variable E which runs from $\alpha - 2\beta$ to $\alpha + 2\beta$. The DOS of the $v = 1$ vibration is then

$$\rho(E) = \frac{1}{2\beta \sin \arccos\left(\frac{\alpha - E}{2\beta}\right)}. \tag{29}$$

This result has been verified by numerical simulations as shown in Fig. 4. The DOS is symmetric around $E = \alpha$, and has no singularities, except at the edges $E = \alpha \pm 2\beta$.

2. Overtone vibration v=2

The spectrum and density of states of the overtone vibration can be calculated analytically only in the harmonic limit. The energies of the $v = 2$ vibrations are

$$E_{k,k'} = 2\alpha - 2\beta(\cos\theta_k + \cos\theta_{k'}), \quad k \leqslant k', \quad k,k' = 1,\ldots,n$$

$$\theta_k = \frac{k\pi}{(n+1)}. \tag{30}$$

For n large, one can introduce two continuous variables $x = \frac{k\pi}{n+1}$ and $y = \frac{k'\pi}{n+1}$ and rewrite Eq. (30) as

$$E(x,y) = 2\alpha - 2\beta(\cos x + \cos y) \tag{31}$$

with $y \geqslant x$. The DOS can be calculated from Eq. (31) using the method introduced by Bowers and Rosenstock [33] and discussed in detail in Sec. IV A 1, yielding

$$g(\tilde{E}) = \frac{4K\left(k_1^2\right)}{\pi^2}, \quad k_1^2 = 4(1 - \tilde{E})\tilde{E}, \tag{32}$$

where K is a complete elliptic integral of the first kind and $\tilde{E} = (E - 2\alpha + 4\beta)/(8\beta), 0 \leqslant \tilde{E} \leqslant 1$. This DOS has a logarithmic singularity at $\tilde{E} = \frac{1}{2}$. This result is confirmed by numerical

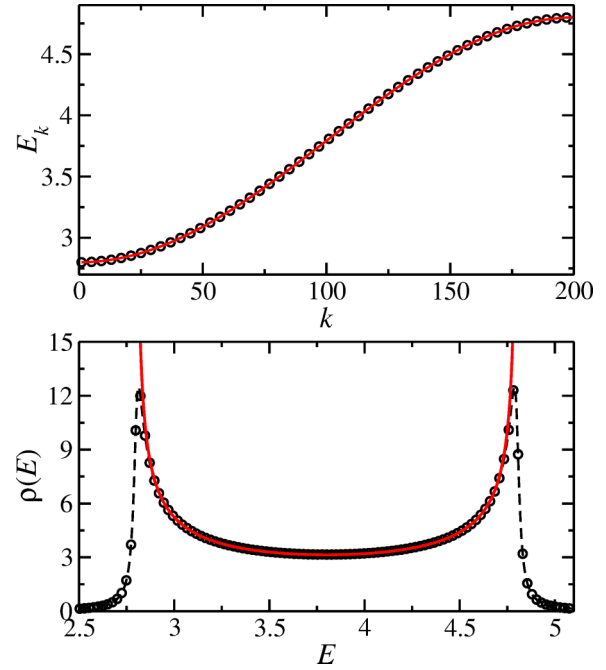FIG. 4. (Color online) EDR and DOS of the $v = 1$ vibration of a linear chain with $v = 1, \lambda = 0.5, A = -1, n = 200, N = 20\,000$. Full red lines: upper panel: Eq. (27), lower panel: Eq. (29).

simulations as shown in Fig. 5 where the energy eigenvalues are plotted as a function of the single index k which labels the eigenvalues in successive order, instead of the double indices k,k' used in Eq. (30).
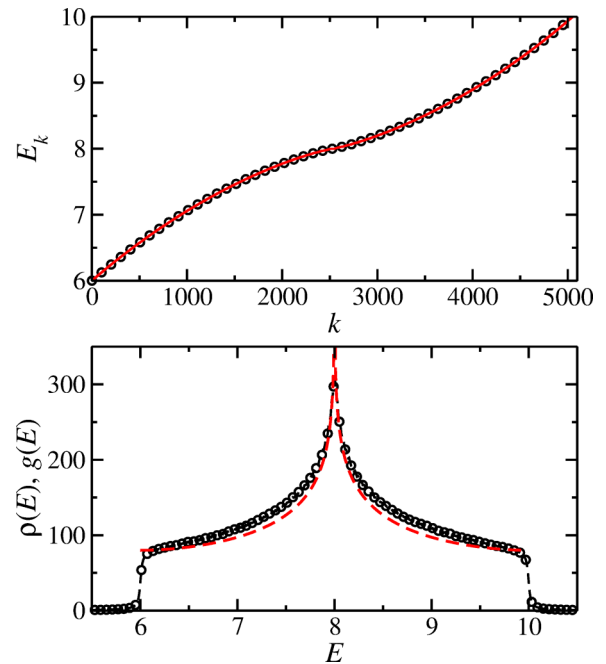

FIG. 5. (Color online) EDR and DOS of the $v = 2$ vibration of a linear chain in the harmonic limit with $\lambda = 0.5, A = -1, n = 100, N = 20\,000$. Full red lines: upper panel: Eq. (30), lower panel: Eq. (32).
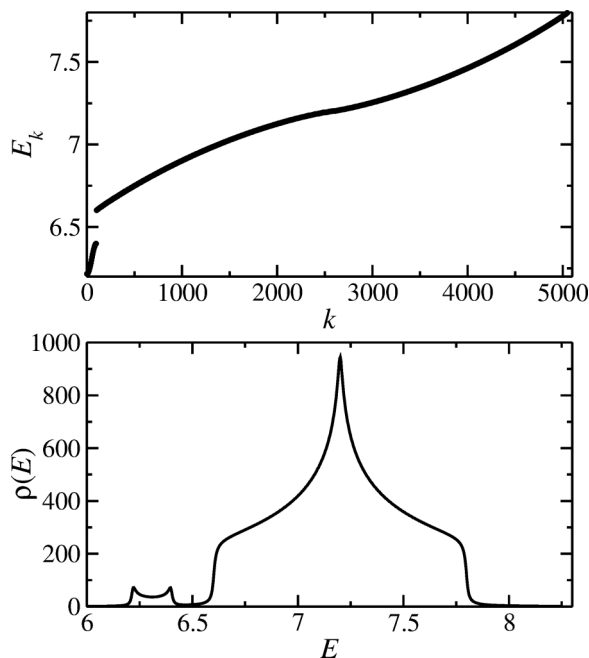
FIG. 6. EDR and DOS of the $v = 2$ vibration of a linear anharmonic chain with $\lambda = 0.15$, $A = -1$, $n = 100$, $N = 10$. The EDR exhibits a gap between $E_k = 6.4$ and 6.6 and, accordingly, the DOS vanishes there.

For anharmonic vibrations, analytic solutions are only available for weak $\frac{\lambda}{A} \ll 1$ and strong $\frac{\lambda}{A} \gg 1$ couplings [29]. Numerical simulations are shown in Fig. 6. The EDR exhibits a gap between $E_k = 6.4$ and 6.6, where the lower sequence contains n eigenvalues and the upper one $n(n-1)/2$ [see Eq. (19)]. The DOS has two edge singularities below the gap and one logarithmic singularity above it.

IV. SQUARE LATTICE

For 2D lattices, the DOS depends on the symmetry of the lattice. We consider first the EDR and DOS of a square lattice.

A real-space cell of this lattice is shown in Fig. 7 left. In this unit cell, there are two and only two types of
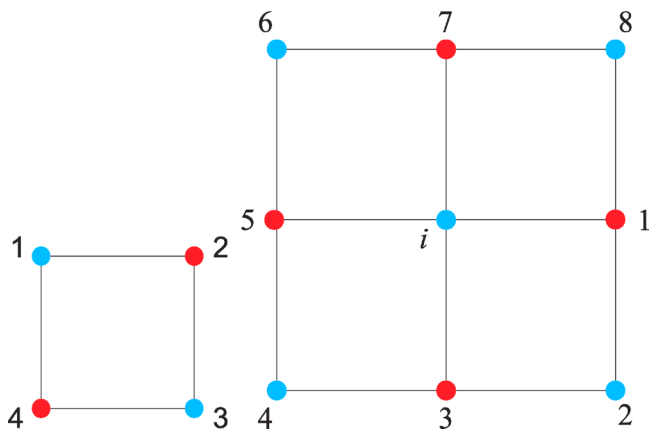

FIG. 7. (Color online) The unit cell (left) and supercell (right) of a square lattice.

interaction: nearest-neighbor and next-to-nearest neighbor. For identical atoms, the symmetry of the unit cell D_{4h} imposes the conditions

$$
\begin{aligned}
\lambda^{(I)} &= \lambda_{12} = \lambda_{23} = \lambda_{34} = \lambda_{41}, \\
\lambda^{(II)} &= \lambda_{13} = \lambda_{24}.
\end{aligned}
\tag{33}
$$

A real-space supercell of this lattice is shown in Fig. 7 right. It consists of four unit cells. The central atom i can interact either with its four nearest neighbors 1, 3, 5, 7, or with its four next-to-nearest neighbors 2, 4, 6, 8. The coordinates of the four nearest neighbors are given by

$$
\frac{\delta_1}{a} = (1,0), \ \frac{\delta_3}{a} = (0,-1), \ \frac{\delta_5}{a} = (-1,0), \ \frac{\delta_7}{a} = (0,1), \tag{34}
$$

while those of the next-to-nearest neighbors are

$$
\frac{\delta_2}{a} = (1,1), \ \frac{\delta_4}{a} = (1,-1), \ \frac{\delta_6}{a} = (-1,-1), \ \frac{\delta_8}{a} = (-1,1), \tag{35}
$$

where a is the lattice constant. The symmetry of the lattice imposes the conditions

$$
\begin{aligned}
\lambda^{(I)} &= \lambda_{i1} = \lambda_{i3} = \lambda_{i5} = \lambda_{i7}, \\
\lambda^{(II)} &= \lambda_{i2} = \lambda_{i4} = \lambda_{i6} = \lambda_{i8}.
\end{aligned}
\tag{36}
$$

The Majorana interaction can then be written as

$$
M = \lambda^{(I)} \sum_{\langle i,j \rangle} M_{ij}^{(I)} + \lambda^{(II)} \sum_{\langle\langle i,j \rangle\rangle} M_{ij}^{(II)}. \tag{37}
$$

In the harmonic limit

$$
M = \lambda^{(I)} \sum_{\langle i,j \rangle} (b_i^\dagger b_j + \text{H.c.}) + \lambda^{(II)} \sum_{\langle\langle i,j \rangle\rangle} (b_i^\dagger b_j + \text{H.c.}). \tag{38}
$$

The full Hamiltonian for n atoms in a square lattice is

$$
\begin{aligned}
H = E_0 &+ A \sum_i C_i + A' \sum_{i<j} C_{ij}' + \lambda^{(I)} \sum_{\langle i,j \rangle} M_{i,j}^{(I)} \\
&+ \lambda^{(II)} \sum_{\langle\langle i,j \rangle\rangle} M_{i,j}^{(II)}.
\end{aligned}
\tag{39}
$$

The operators

$$
\sum_{\langle i,j \rangle} M_{ij}^{(I)} \equiv S^{(I)}, \quad \sum_{\langle\langle i,j \rangle\rangle} M_{ij}^{(II)} \equiv S^{(II)} \tag{40}
$$

are also called symmetry adapter operators.

A. Solutions

1. Fundamental vibration v=1

The EDR and the DOS of the fundamental vibration $v = 1$ of a square lattice with nearest-neighbor and next-to-nearest-neighbor interactions and Hamiltonian (38) can be obtained analytically by purely algebraic methods by making use of certain properties of matrices as discussed in Sec. III A 1, Eqs. (25) and (26).

The Hamiltonian matrix is obtained by taking matrix elements of H, Eq. (39), in the basis $|1,0,0,\ldots\rangle, |0,1,0,\ldots\rangle, \ldots, |0,0,\ldots,0,1\rangle \equiv |1_j\rangle$ of Eq. (19). The operators C_i, C_{ij}'

are diagonal in this basis with values given by $-4(1 - \frac{1}{N})$ and $-4(\frac{1}{2N})$ [Eq. (11)]. The interesting operators are $S^{(I)}$ and $S^{(II)}$. The matrices representative of these operators are of the type discussed previously and thus can be diagonalized analytically. The solution for the fundamental vibration of a square lattice was first given by Bowers and Rosenstock [33] in terms of functions over an area and subsequently by Nierenberg [31] in terms of functions over a line. In Ref. [33], the eigenvalues of $S^{(I)}$ and $S^{(II)}$ are labeled by two integers $p, q = 1, 2, \ldots, n$ and given by

$$m^{(I)}(p,q) = 2\left(\cos\frac{p\pi}{n+1} + \cos\frac{q\pi}{n+1}\right),$$
$$m^{(II)}(p,q) = 4\left(\cos\frac{p\pi}{n+1}\cos\frac{q\pi}{n+1}\right). \quad (41)$$

From these, one can construct the eigenvalues of the Majorana operator $M = \lambda^{(I)} S^{(I)} + \lambda^{(II)} S^{(II)}$ as

$$m(p,q) = \lambda^{(I)} 2\left(-\cos\frac{p\pi}{n+1} - \cos\frac{q\pi}{n+1}\right)$$
$$+ \lambda^{(II)} 4\left(-\cos\frac{p\pi}{n+1}\cos\frac{q\pi}{n+1}\right), \quad (42)$$

where the minus sign has been introduced to conform with the definition in Eq. (13). These solutions can be easily verified for the unit cell $n = 4$, and for the supercell $n = 9$. For the unit cell $n = 4$, the eigenvalues are given in the terms of $\cos(\frac{p\pi}{3})$ and are

$$
\begin{aligned}
(I): \quad &\pm 2, 0, 0, \\
(II): \quad &\pm 1, \pm 1.
\end{aligned}
\quad (43)
$$

For the supercell $n = 9$, they are

$$
\begin{aligned}
(I): \quad &\pm 2\sqrt{2}, \pm\sqrt{2}, \pm\sqrt{2}, 0, 0, 0, \\
(II): \quad &\pm 2, \pm 2, 0, 0, 0, 0, 0.
\end{aligned}
\quad (44)
$$

For the unit cell, the eigenstates are representations of D_{4h}. The eigenstates of (I) are the singly degenerate representations A, B and the doubly degenerate representation E [34].

When n is very large, one may replace $\frac{p\pi}{n+1}$ and $\frac{q\pi}{n+1}$ by continuous variables x and y, respectively, which run from 0 to π:

$$m(x,y) = \lambda^{(I)} 2(-\cos x - \cos y)$$
$$+ \lambda^{(II)} 4(-\cos x \cos y), \quad 0 \leqslant x, y \leqslant \pi. \quad (45)$$

The DOS can be obtained from Eq. (45). For purposes of display, it is convenient to consider the shifted function [33]

$$f(x,y) = \lambda^{(I)} 2(2 - \cos x - \cos y)$$
$$+ \lambda^{(II)} 4(1 - \cos x \cos y), \quad 0 \leqslant x, y \leqslant \pi. \quad (46)$$

The DOS $g(E)$ is obtained from Eq. (45) by

$$g(E) = \frac{1}{\pi^2} \int_0^\pi \int_0^\pi \delta[E - f(x,y)] dx \, dy. \quad (47)$$

The DOS is particularly simple when $\lambda^{(II)}/\lambda^{(I)} \leqslant \frac{1}{2}$. In this case, introducing $E_{\max} = 8\lambda^{(I)}$ and $\tilde{E} = E/E_{\max}$, it can
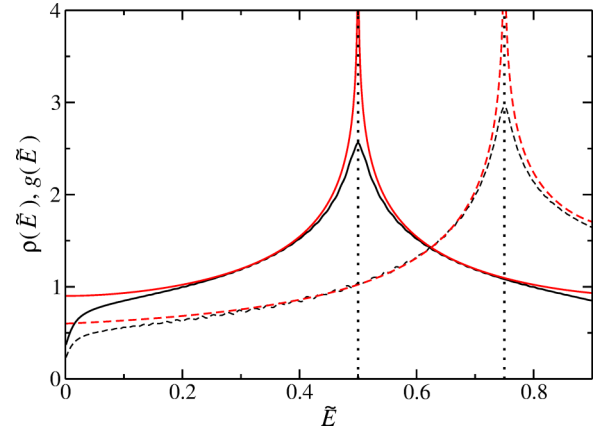

FIG. 8. (Color online) Black: DOS of the fundamental vibration $v = 1$ of a square lattice with $n = 2500$, $A = -1$, $N = 20000$. Full lines: $\lambda^{(II)}/\lambda^{(I)} = 0$. Dashed lines: $\lambda^{(II)}/\lambda^{(I)} = 0.25$. Red: Eq. (49).

be written in terms of an elliptic integral:

$$g(\tilde{E}) = \frac{4K(k_1^2)}{\pi^2\sqrt{(1 + 2\lambda^{(II)}/\lambda^{(I)})^2 - 8(\lambda^{(II)}/\lambda^{(I)})\tilde{E}}},$$
$$k_1^2 = \frac{4(1 - \tilde{E})\tilde{E}}{(1 + 2\lambda^{(II)}/\lambda^{(I)})^2 - 8(\lambda^{(II)}/\lambda^{(I)})^2\tilde{E}}, \quad 0 < \tilde{E} < 1. \quad (48)$$

For nearest-neighbor interactions $\lambda^{(II)} = 0$, the DOS takes the form

$$g(\tilde{E}) = \frac{4K(k_1^2)}{\pi^2}, \quad k_1^2 = 4(1 - \tilde{E})\tilde{E}, \quad (49)$$

which is symmetric around $\tilde{E} = \frac{1}{2}$. The DOS $g(\tilde{E})$ is shown in Fig. 8 for purely nearest-neighbor interactions $\lambda^{(II)} = 0$ and next-to-nearest-neighbor interactions, with $\lambda^{(II)} = \frac{1}{4}\lambda^{(I)}$.

From this "reduced" DOS, one can reconstruct the "true" DOS. The energy of the $v = 1$ states including the diagonal terms is given by

$$E(p,q) = E_0 - 4A\left(1 - \frac{1}{N}\right) - 4A'\left(\frac{1}{2N}\right) + m(p,q). \quad (50)$$

The true DOS is obtained from Eq. (46) by changing $\tilde{E}$ to $E = 8\lambda^{(I)}\tilde{E}$ and shifting it by the amount $E_0 - 4A(1 - \frac{1}{N}) - 4A'(\frac{1}{2N}) - 4\lambda^{(I)} - 4\lambda^{(II)}$. It is interesting to note that the structure of the DOS is a consequence of the symmetry D_{4h} of the unit cell, and is already encoded into the DOS of the unit cell and the supercell, as shown in Fig. 9.

This result has been verified by numerical simulations as shown in Fig. 10. The DOS of the $v = 1$ vibration of a square lattice has a logarithmic singularity at $\tilde{E} = \frac{1}{2}$.

It should be noted that the DOS of the fundamental vibration $v = 1$ of the 2D lattice is identical to that of the overtone vibration $v = 2$ of the 1D lattice. This result follows from the mapping of the function $f(x,y)$ defined over an area onto a function defined over a line, as discussed by Nierenberg [31].

2. Overtone v=2

While for the fundamental vibration $v = 1$ the EDR and the DOS do not depend on whether or not the crystal is harmonic, for the overtone $v = 2$ they do. The spectrum of states can be
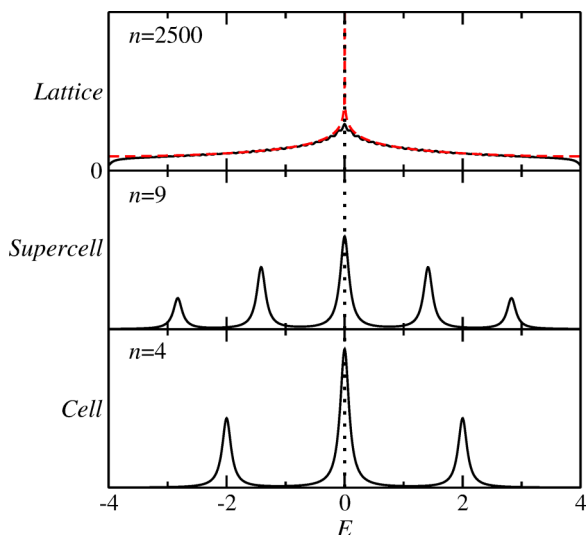
FIG. 9. (Color online) DOS of the fundamental vibration $v = 1$ of a square lattice including the unit cell and the supercell with the number of sites n as indicated in the insets. Red dashed line: Eq. (49).

calculated by diagonalizing the Hamiltonian H in the basis $|2,0,0,\ldots\rangle$, $|1,1,0,\ldots\rangle$, $|1,0,1,\ldots\rangle$, $\ldots$ of Eq. (19), with in total two quanta, in terms of the four parameters A, A', $\lambda^{(I)}$, $\lambda^{(II)}$ and the anharmonicity parameter N. Analytic solutions can be obtained only in the weak coupling ($\lambda/A \ll 1$) and strong coupling limit ($\lambda/A \gg 1$) [29,32].

In order to illustrate the properties of the solutions, we consider the case of a highly anharmonic vibration with $N = 10$, $-4A = 4$, $-4A' = 0$, and only nearest-neighbor interactions $\lambda^{(I)} = 0.03$, $\lambda^{(II)} = 0$. The DOS of $v = 2$ states
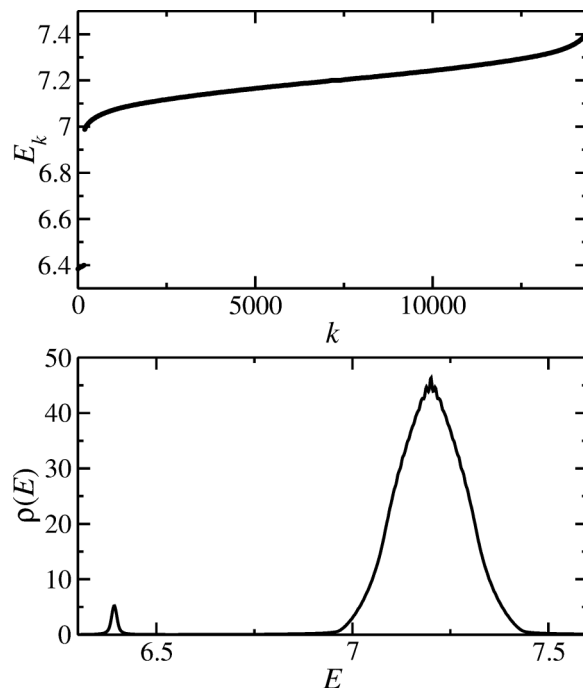

FIG. 11. EDR and DOS of the $v = 2$ overtone of an anharmonic square lattice with $n = 169$, $A = -1$, $N = 10$, $\lambda = 0.03$.

has two parts. Both parts diverge as $n \to \infty$, the first part as n and the second as n^2. This is seen in the numerical simulation in Fig. 11. The splitting into two pieces containing n and $n(n-1)/2$ eigenvalues, respectively, can already be seen in the unit cell, $n = 4$, and in the supercell, $n = 9$, as shown in Fig. 12.

V. HONEYCOMB LATTICE

A real-space cell of this lattice is shown in the left part of Fig. 13. In this unit cell, there are three and only three types of

FIG. 10. (Color online) EDR and DOS of the fundamental vibration $v = 1$ of a harmonic square lattice with $n = 2500$, $A = -1$, $N = 20000$, $\lambda^{(I)} = 0.5$, $\lambda^{(II)} = 0$. Red lines: Eq. (49).
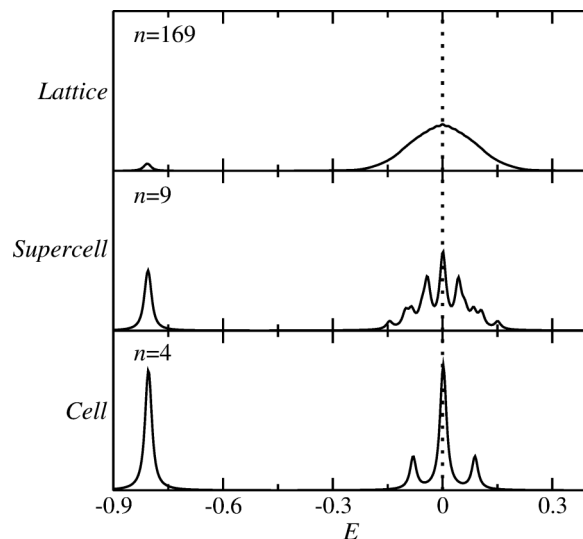

FIG. 12. DOS of the $v = 2$ overtone of an anharmonic square lattice including the unit cell and the supercell with the number of sites indicated in the insets and $A = -1$, $N = 10$, $\lambda = 0.03$.
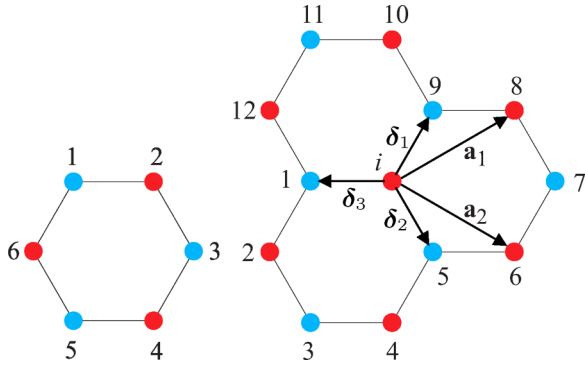
FIG. 13. (Color online) The unit cell of the honeycomb lattice (left) and its supercell (right).

interaction, (I) nearest neighbor, (I) next-to-nearest neighbor, and (III) third neighbor. For identical atoms the symmetry of the unit cell D_{6h} imposes the condition ([23], p. 139) for the interactions

$$\lambda^{(I)} = \lambda_{12} = \lambda_{23} = \lambda_{34} = \lambda_{45} = \lambda_{56} = \lambda_{16},$$
$$\lambda^{(II)} = \lambda_{13} = \lambda_{24} = \lambda_{35} = \lambda_{46} = \lambda_{15} = \lambda_{26}, \quad (51)$$
$$\lambda^{(III)} = \lambda_{14} = \lambda_{25} = \lambda_{36}.$$

A real-space supercell of this lattice is shown in Fig. 13 right. It consists of three unit hexagonal cells. The central atom i can interact either with its three nearest neighbors 1, 5, 9, or with its six next-to-nearest neighbors 2, 4, 6, 8, 10, 12, or with its three third neighbors 3, 7, 10. The coordinates of the nearest neighbors are given by

$$\boldsymbol{\delta}_1 = \frac{a}{2}(1, \sqrt{3}), \ \boldsymbol{\delta}_2 = \frac{a}{2}(1, -\sqrt{3}), \ \boldsymbol{\delta}_3 = -a(1,0), \quad (52)$$

while those of the next-to-nearest neighbor $\boldsymbol{\delta}'$ and third neighbor $\boldsymbol{\delta}''$ are given in terms of the lattice vectors

$$\boldsymbol{a}_1 = \frac{a}{2}(3, \sqrt{3}), \ \boldsymbol{a}_2 = \frac{a}{2}(3, -\sqrt{3}) \quad (53)$$

as

$$\boldsymbol{\delta}'_1 = \pm\boldsymbol{a}_1, \ \boldsymbol{\delta}'_2 = \pm\boldsymbol{a}_2, \ \boldsymbol{\delta}'_3 = \pm(\boldsymbol{a}_2 - \boldsymbol{a}_1), \quad (54)$$
$$\boldsymbol{\delta}''_1 = \boldsymbol{a}_1 + \boldsymbol{\delta}_2, \ \boldsymbol{\delta}''_2 - \boldsymbol{a}_1 + \boldsymbol{\delta}_2, \ \boldsymbol{\delta}''_3 = -\boldsymbol{a}_2 + \boldsymbol{\delta}_1.$$

The symmetry of the unit cell of the honeycomb lattice D_{6h} imposes the conditions

$$\lambda^{(I)} = \lambda_{i1} = \lambda_{i5} = \lambda_{i9},$$
$$\lambda^{(II)} = \lambda_{i2} = \lambda_{i4} = \lambda_{i6} = \lambda_{i8} = \lambda_{i10} = \lambda_{i12}, \quad (55)$$
$$\lambda^{(III)} = \lambda_{i3} = \lambda_{i7} = \lambda_{i10}.$$

The Majorana interaction for the honeycomb lattice can be written as

$$M = \lambda^{(I)} \sum_{\langle i,j \rangle} M_{ij}^{(I)} + \lambda^{(II)} \sum_{\langle\langle i,j \rangle\rangle} M_{ij}^{(II)}$$
$$+ \lambda^{(III)} \sum_{\langle\langle\langle i,j \rangle\rangle\rangle} M_{ij}^{(III)}. \quad (56)$$

In the harmonic limit, M becomes the Hamiltonian of the tight-binding model [3]

$$M = \lambda^{(I)} \sum_{\langle i,j \rangle} (b_i^\dagger b_j + \text{H.c.}) + \lambda^{(II)} \sum_{\langle\langle i,j \rangle\rangle} (b_i^\dagger b_j + \text{H.c.})$$
$$+ \lambda^{(III)} \sum_{\langle\langle\langle i,j \rangle\rangle\rangle} (b_i^\dagger b_j + \text{H.c.}). \quad (57)$$

The honeycomb lattice can also be viewed as two interpenetrating triangular lattices A and B [21]. In the unit cell shown in the left part of Fig. 13, the three atoms 1, 5, 9 belong to A and the three atoms 2, 4, 6 belong to B. Neglecting third-neighbor interactions, denoting by $a_i^\dagger$ and $b_i^\dagger$ the boson creation operators at site i on sublattices A and B, Eq. (42) can be rewritten as

$$M = -t \sum_{\langle i,j \rangle} (a_i^\dagger b_j + \text{H.c.}) - t' \sum_{\langle\langle i,j \rangle\rangle} (a_i^\dagger a_j + b_i^\dagger b_j + \text{H.c.}), (58)$$

where $t = \lambda^{(I)}$ and $t' = \lambda^{(II)}$.

The Majorana operator in Eq. (57) is written in terms of boson operators. Its structure, however, depends only on the symmetry of the lattice. The symmetry adaptation in Eq. (57) can therefore also be used for fermions. Introducing fermion creation operators $a_{i,\sigma}^\dagger, b_{i,\sigma}^\dagger$, the Hamiltonian has the form

$$M = -t \sum_{\langle i,j \rangle, \sigma} (a_{\sigma,i}^\dagger b_{\sigma,j} + \text{H.c.})$$
$$- t' \sum_{\langle\langle i,j \rangle, \sigma\rangle} (a_{\sigma,i}^\dagger a_{\sigma,j} + b_{\sigma,i}^\dagger b_{\sigma,j} + \text{H.c.}), \quad (59)$$

describing electrons that can hop from one site to the other in the interpenetrating triangular lattices A and B [3]. The problem of transverse vibrations of a honeycomb lattice is thus formally identical to that of the band structure of the lattice, except for the replacement of boson operators by fermion operators. The only difference is that while for bosons one can put any number at each site, for fermions one can put only one at each site (or two if one takes into account the spin).

The full algebraic Hamiltonian for vibrations of the honeycomb lattice is

$$H = E_0 + A \sum_i C_i + A' \sum_{i \neq j} C'_{i,j} + \lambda^{(I)} \sum_{\langle i,j \rangle} M_{i,j}^{(I)}$$
$$+ \lambda^{(II)} \sum_{\langle\langle i,j \rangle\rangle} M_{ij}^{(II)} + \lambda^{(III)} \sum_{\langle\langle\langle i,j \rangle\rangle\rangle} M_{ij}^{(III)}. \quad (60)$$

There are therefore for this problem three symmetry adapter operators

$$S^{(I)} = \sum_{\langle i,j \rangle} M_{ij}^{(I)}, \ S^{(II)} = \sum_{\langle\langle i,j \rangle\rangle} M_{ij}^{(II)},$$
$$S^{(III)} = \sum_{\langle\langle\langle i,j \rangle\rangle\rangle} M_{ij}^{(III)}.$$

A. Solutions

1. Fundamental vibration v=1

The eigenvalues of the symmetry adapter operators $S^{(I)}$, $S^{(II)}$, and $S^{(III)}$ for the unit cell are given by

$$
\begin{aligned}
(I): &\quad \pm 2, \pm 1, \pm 1, \\
(II): &\quad \pm 2, \pm 1, \pm 1, \\
(III): &\quad \pm 1, \pm 1, \pm 1,
\end{aligned}
\tag{61}
$$

while for the supercell they are given by

$$
\begin{aligned}
(I): &\ \pm 2.3810, \pm 1.7320, \pm 1.5735, \pm 1, \pm 1, \pm 0.9246, 0, \\
(II): &\ 3.6457, 3.0861, 1, 1, 0.618, 0.428, \\
&\ -1, -1, -1, -1.514, -1.618, -1.645, -2, \\
(III): &\ \pm\sqrt{2}, \pm\sqrt{2}, \pm 1, \pm 1, 0, 0.0, 0.0.
\end{aligned}
\tag{62}
$$

The eigenstates are representations of D_{6h} [34]. When the number of cells is very large, an analytic solution was given by Wallace [21] who solved the equivalent problem of fermions on the honeycomb lattice (see also [22]):

$$
\begin{aligned}
E(k_x, k_y) &= \gamma_0 E^{(I)}(k_x, k_y) + \gamma_1 E^{(II)}(k_x, k_y), \\
E^{(I)}(k_x, k_y) &= \pm\sqrt{3 + u(k_x, k_y)}, \\
E^{(II)}(k_x, k_y) &= -u(k_x, k_y), \\
u(k_x, k_y) &= 2\cos 2\pi k_y a + 4\cos \pi k_y a \cos \pi k_x \sqrt{3}a,
\end{aligned}
\tag{63}
$$

where $\pi k_x a = x$ and $\pi k_y a = y$ are continuous variables. The Hamiltonian used by Wallace differs from M by a constant (a shift in E). Hobson and Nierenberg [35] using a method similar to that described in Sec. IV A 1 for the square lattice provided an analytic expression for the DOS for nearest-neighbor interactions. Introducing $E_{\max} = 6\lambda^{(I)}$ and $\tilde{E} = E/E_{\max}$, $-1 < \tilde{E} < 1$, $\omega = (\tilde{E} + 1)/2$, the DOS is given in terms of an elliptic integral

$$
\begin{aligned}
g(\omega) &= \frac{9}{\pi^2}\sqrt{\frac{1-2\omega}{3}} K\left(\sqrt{\frac{\omega(2-3\omega)^3}{(1-2\omega)}}\right), \quad 0 < \omega < \frac{1}{3} \\
g(\omega) &= \frac{9}{\pi^2}\frac{(1-2\omega)}{\sqrt{3\omega(2-3\omega)^3}} K\left(\sqrt{\frac{1-2\omega}{\omega(2-3\omega)^3}}\right), \quad \frac{1}{3} \leqslant \omega \leqslant \frac{1}{2}
\end{aligned}
\tag{64}
$$

and the function is symmetric around $\omega = \frac{1}{2}$, i.e., around $\tilde{E} = 0$ (see Fig. 14).

The Hamiltonian used by Hobson and Nierenberg differs from M, and from the Hamiltonian of Wallace by a constant. The DOS Eq. (64) should be compared with that of a square lattice, given by Eq. (49). The difference between the two is a consequence of the symmetry of the lattice. The major difference between the two DOSs is the occurrence of a zero (Dirac zero) at $\tilde{E} = 0$ in the honeycomb lattice. The properties of the DOS of the honeycomb lattice are due to the symmetry D_{6h} of the unit cell and are already encoded into the DOS of the unit cell and the supercell, as shown in Fig. 15.

These results have been verified by numerical simulations as shown in Fig. 16. For finite n a peak occurs at $E = 0$, which is due to the presence of zigzag edges in the lattice structure [36].
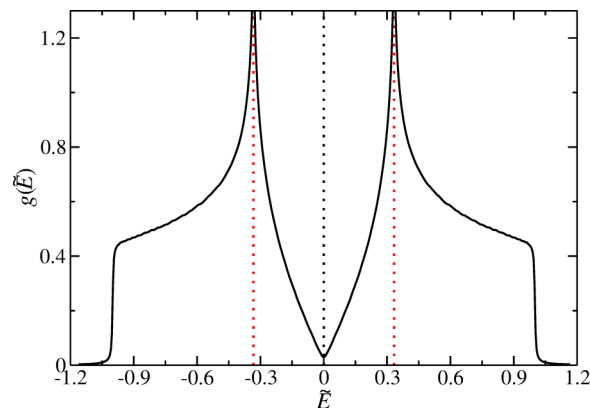

FIG. 14. (Color online) The DOS of the $v = 1$ vibration of the honeycomb lattice [Eq. (64)].

2. Overtone v=2

The spectrum (EDR) and density of states (DOS) can also be calculated by diagonalizing the Hamiltonian H of Eq. (57) in the space $v = 2$, $|2,0,0,\ldots\rangle$, $|1,1,0,\ldots\rangle$, $|1,0,1,0,\ldots\rangle$, $\ldots$, in terms of the five parameters A, A', $\lambda^{(I)}$, $\lambda^{(II)}$, $\lambda^{(III)}$ and the anharmonicity parameter N. In order to illustrate the properties of the solutions, we consider the case of a highly anharmonic vibration with $N = 10$, $-4A = 4$, $-4A' = 0$, and only nearest-neighbor interactions $\lambda^{(I)} = 0.03$, $\lambda^{(II)} = \lambda^{(III)} = 0$. Also here the DOS of $v = 2$ has two parts, as shown in Fig. 17. The first part diverges as n and has only edge singularities as illustrated in Fig. 18, the second part diverges as n^2, and has a logarithmic singularity and two shoulders. The splitting into these two parts can also be seen in the unit cell and in the supercell as shown in Fig. 19.

VI. SUMMARY OF DOS AND EDR

The results of Secs. III–V are summarized in Figs. 20 and 21. For the fundamental vibration $v = 1$, they confirm the
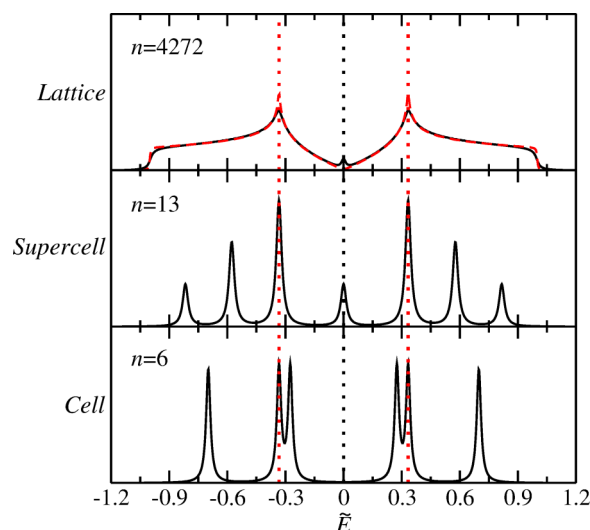

FIG. 15. (Color online) DOS of the fundamental vibration $v = 1$ of the honeycomb lattice including the unit cell and the supercell with the number of sites n as indicated in the insets. Red dashed line: Eq. (64).
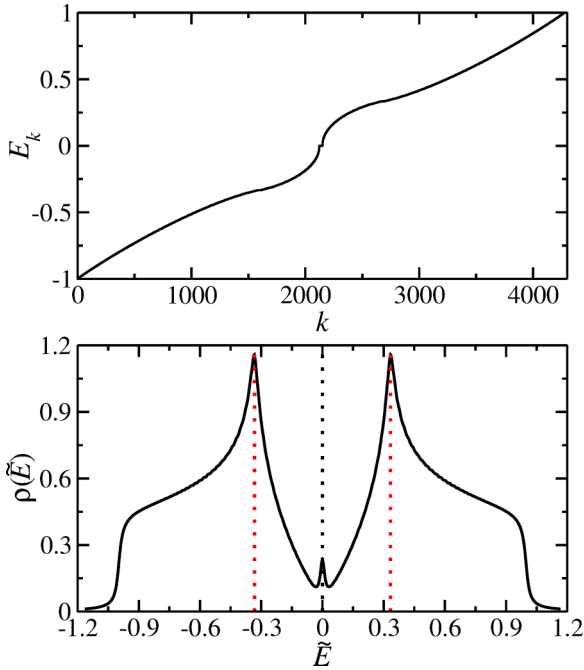
FIG. 16. (Color online) EDR and DOS of the fundamental vibration $v = 1$ of a honeycomb lattice with $n = 4272$ sites.

conjecture of van Hove [37] that singularities in the level density occur only in two dimensions.

VII. ENERGY SURFACES AND PHONON DISPERSION RELATIONS

It is of interest to display explicitly the energy surfaces and phonon dispersion relations of infinite-size lattices. For the square lattice, the energy surface for nearest-neighbor
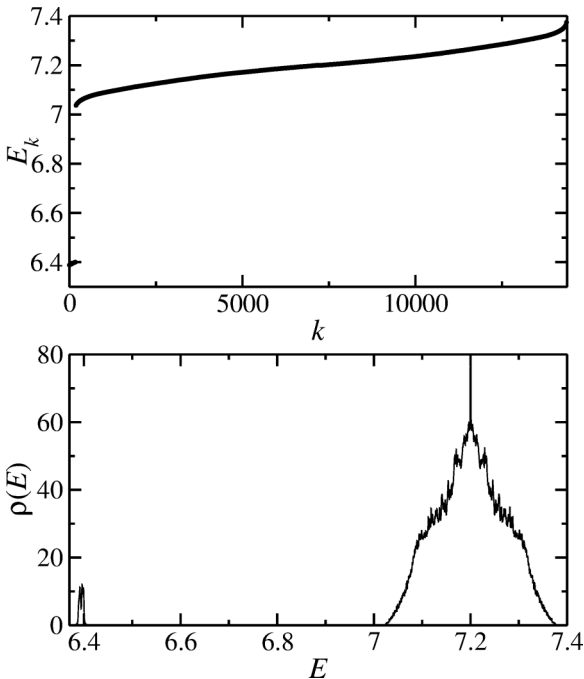

FIG. 17. EDR and DOS of the overtone vibration $v = 2$ of a honeycomb lattice with $n = 169$, $A = -1$, $N = 10$, $\lambda = 0.03$.
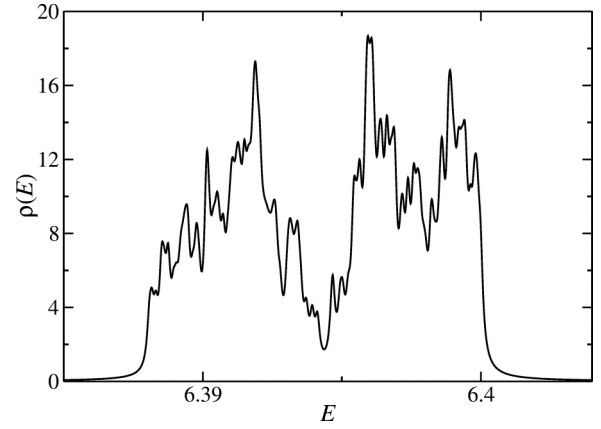
FIG. 18. Zoom into the small peak in the DOS of the overtone vibration $v = 2$ of a honeycomb lattice with $n = 169$, $A = -1$, $N = 10$, $\lambda = 0.03$ shown in Fig. 17.
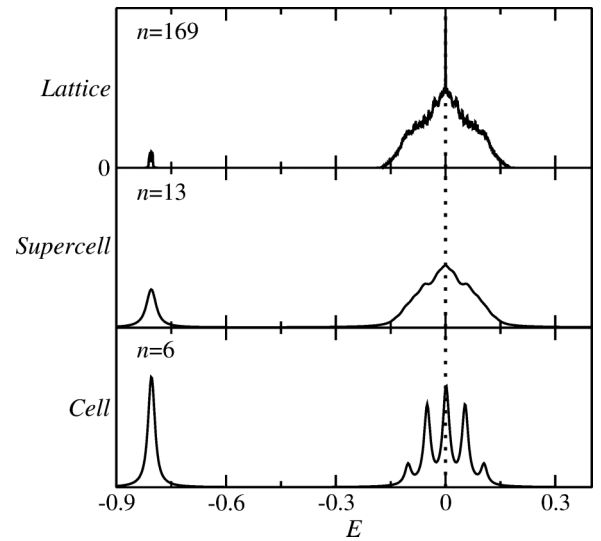

FIG. 19. DOS of the $v = 2$ overtone of a honeycomb lattice including the cell and supercell with the number of sites n indicated in the insets and $A = -1$, $N = 10$, $\lambda = 0.03$.
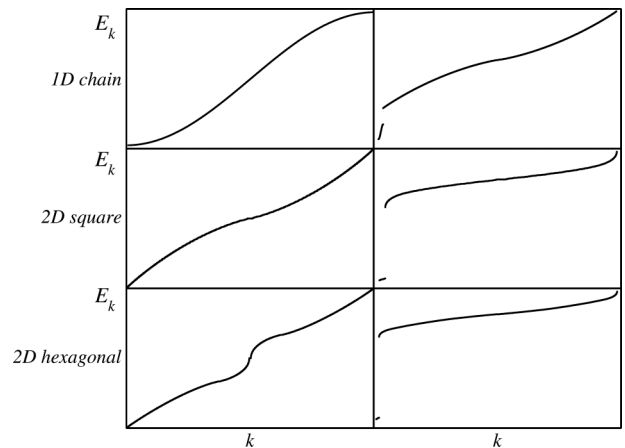

FIG. 20. Summary of the EDRs of transverse crystal vibrations. Left: $v = 1$; right: $v = 2$.
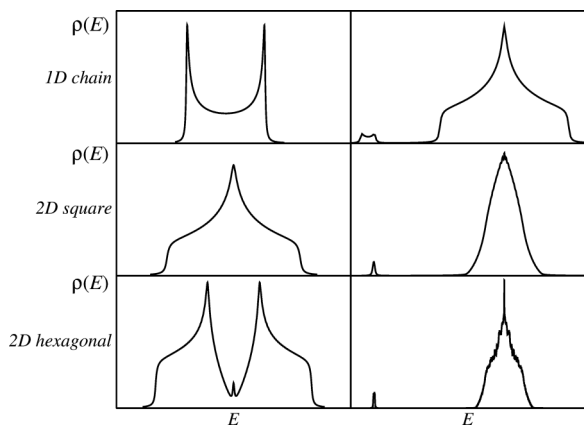
FIG. 21. Same as Fig. 20 for the DOSs.

FIG. 23. Computed phonon dispersion relation of an infinite-size square lattice.

interactions is given by Eq. (46), rewritten, for $2\lambda^{(I)} = 1$, as

$$E(k_x, k_y) = (2 - \cos \pi k_x a - \cos \pi k_y a). \quad (65)$$

This energy surface is shown in Fig. 22. The corresponding phonon dispersion relation along the boundary of the first irreducible Brillouin zone is shown in Fig. 23. The special points $\Gamma(0,0)$, $M(\frac{1}{2a},0)$, $X(\frac{1}{2a},\frac{1}{2a})$ are indicated in the density plot, shown in the right part of Fig. 22.

For the hexagonal lattice, the energy surface for nearest-neighbor interaction is given by Eq. (62) rewritten as [3]

$$E(k_x, k_y) = \pm\sqrt{3 + f(k_x, k_y)},$$
$$\quad (66)$$
$$f(k_x, k_y) = 2\cos\left(\sqrt{3}k_y a\right) + 4\cos\left(\frac{\sqrt{3}}{2}k_y a\right)\cos\left(\frac{3}{2}k_x a\right).$$

This energy surface is shown in Fig. 24. Because of the $\pm$ sign in Eq. (66), it consists of two sheets which touch conically at the corners of the first Brillouin zone. This $\pm$ sign is a consequence of the fact that the hexagonal lattice can be viewed as two interpenetrating triangular lattices as discussed in Sec. V. This is the crucial property that makes the hexagonal lattice so different from other lattices. The phonon dispersion relation is shown in Fig. 25. The special points $\Gamma(0,0)$, $M(\frac{2\pi}{3a},0)$, $K(\frac{2\pi}{3a},\frac{2\pi}{3\sqrt{3}a})$ are indicated in the density plot,

shown in the right part of Fig. 24. In Figs. 22 and 24, one can see clearly the symmetry of the unit cells D_{4h} (square) and D_{6h} (hexagonal).

As mentioned in Sec. V, the structure of the algebraic Hamiltonian applies to both bosons and fermions, and it depends only on the symmetry of the lattice. Thus, the energy surfaces and dispersion relations (65) and (66) apply also to electrons in a square and hexagonal lattice. In this case, $\boldsymbol{k} = (k_x, k_y)$ represents the quasimomentum of electrons. This is what makes graphene so special.

VIII. COMPARISON WITH DATA IN MICROWAVE PHOTONIC CRYSTALS

Superconducting microwave resonators have been used for two decades as analog systems for the study of quantum phenomena in high-resolution measurements [6,8,9,38]. Photonic crystals are the optical analog of a solid. Both concepts can be combined into "microwave photonic crystals" which offer the opportunity to perform high-precision measurements of the excitation spectrum, and thus to study the EDR and DOS of solids. In particular, recently two-dimensional hexagonal structures were realized by squeezing a photonic
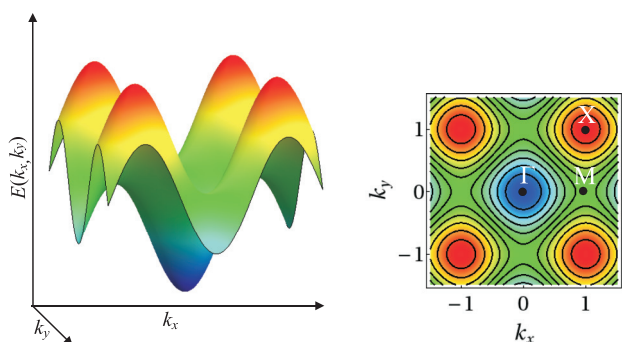

FIG. 22. (Color online) The left panel shows the energy surface of the $v = 1$ vibrations [Eq. (65)] of an infinite-size square lattice, where the lattice constant a was set to unity. The right panel shows the corresponding density plot in the quasimomentum plane (k_x, k_y) with the isofrequency lines shown as dark lines.
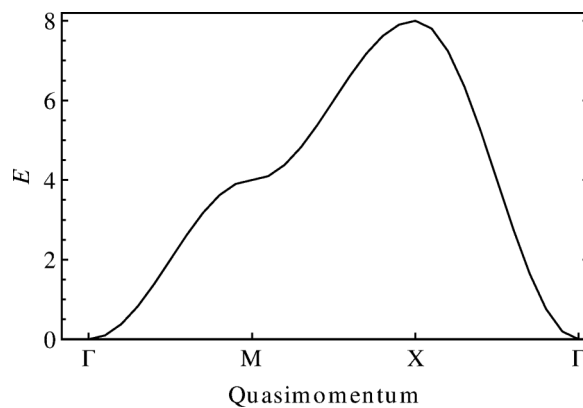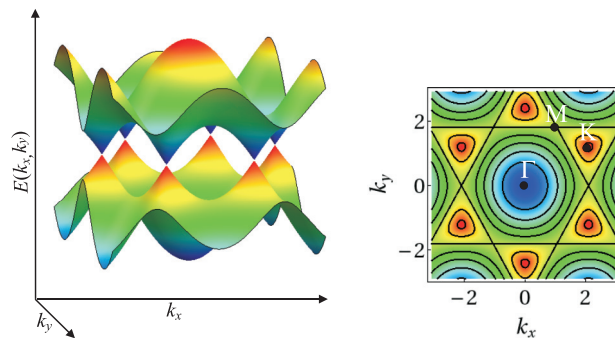

FIG. 24. (Color online) The left panel shows the two sheets of the energy surface of the $v = 1$ vibrations [Eq. (66)] of an infinite-size hexagonal lattice, where a was set to unity. They touch each other conically at the corners of the first Brillouin zone. The right panel shows the corresponding density plot in the quasimomentum plane (k_x, k_y) with the isofrequency lines shown as dark lines.
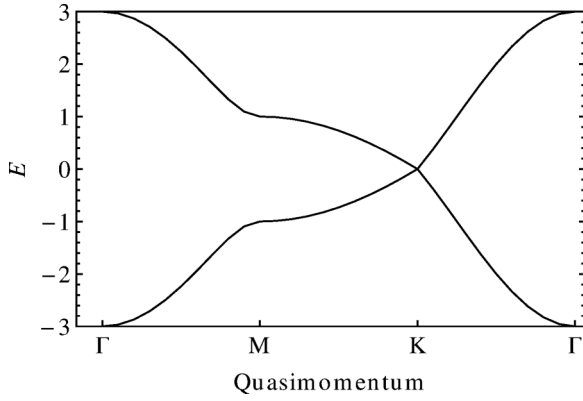
FIG. 25. Computed phonon dispersion relation of an infinite-size hexagonal lattice.

FIG. 27. (Color online) Same as in Fig. 26 but for an Africa billiard. The top plate was removed. Adopted from [38].

crystal, which was composed of several hundreds of metallic cylinders forming a triangular lattice, between two metal plates [20,39,40].

In order to investigate the EDR and the DOS of hexagonal lattices of varying shapes, high-precision experiments were performed with flat, superconducting microwave resonators with the forms of a rectangle and the African continent [41], respectively. Photographs are shown in the left parts of Figs. 26 and 27. Both resonators consisted of a basin and a lid, that were made from brass plates and then lead plated to attain superconductivity at the liquid-helium temperature of 4.2 K. Note that the critical temperature of lead is $T_c = 7.2$ K. For the construction of the photonic crystals located inside the basins ≈ 900 cylinders were milled out of the bottom plate. The cylinders were arranged on a triangular grid, as indicated in the schematic views in Figs. 26 and 27. Then, the voids at the centers of the cells formed by, respectively, three of them yield a hexagonal configuration. The height of the resonators was $h = 3$ mm and the range of excitation frequencies f of the microwaves that were coupled into the resonator was chosen as $0 \leqslant f \leqslant f_{\max} = c/2h$ so the electric field vector was perpendicular to the top and bottom plates of the resonators. Then, the microwaves inside the resonators are governed by the scalar Helmholtz equation for the electric field strength with Dirichlet boundary conditions at the walls of the cylinders and the basin and the microwave photonic crystals correspond to experimental realizations of hexagonal lattices. Consequently, the model (59) should be applicable.
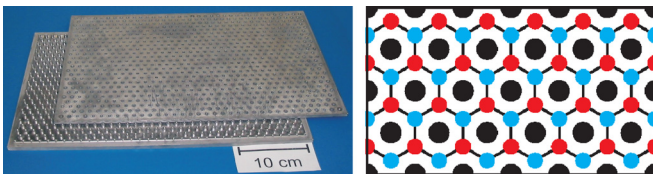

FIG. 26. (Color online) Left part: photograph of the rectangular microwave photonic crystal, which contains 888 metal cylinders arranged on a triangular grid. The top plate was shifted with respect to the bottom one for presentational reasons. Right part: schematic view of the triangular lattice. The red (gray) and blue (dark gray) dots mark the voids between the cylinders that form the hexagonal lattice. Adopted from [38].
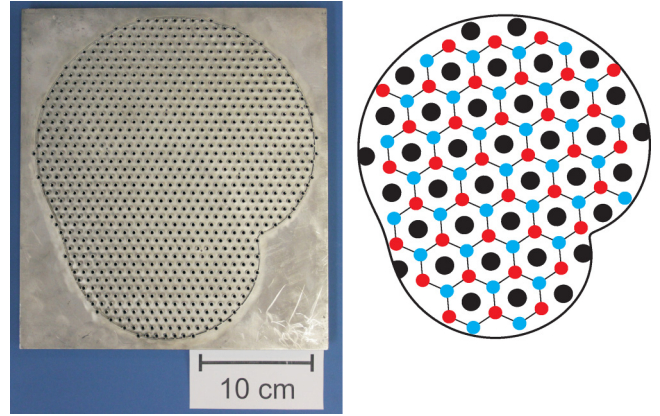
We determined altogether 1651 and 1823 resonance frequencies in the first two bands of the rectangular and the Africa-shaped microwave photonic crystal, respectively. The EDRs, f_k vs k, and the DOSs $\rho(f)$ are shown in Figs. 28 and 29. A fit to the DOS with the algebraic Hamiltonian (60) with nearest-neighbor coupling $\lambda^{(I)}$, and second- and third-neighbor couplings $\lambda^{(II)}$ and $\lambda^{(III)}$ yielded the red dashed curves in Fig. 29. The best fit values are for the rectangular crystal $\lambda^{(I)} = 4.573$ GHz, $\lambda^{(II)} = -0.284$ GHz, $\lambda^{(III)} = 0.104$ GHz,
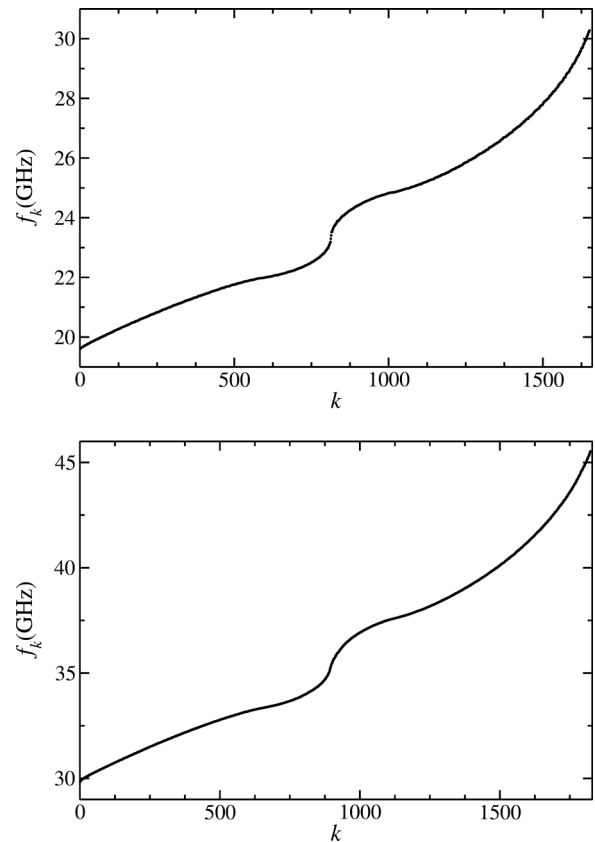

FIG. 28. Experimental EDR for the rectangular photonic crystal with 1656 sites (upper panel) and the Africa-shaped one with 1823 sites (lower panel).
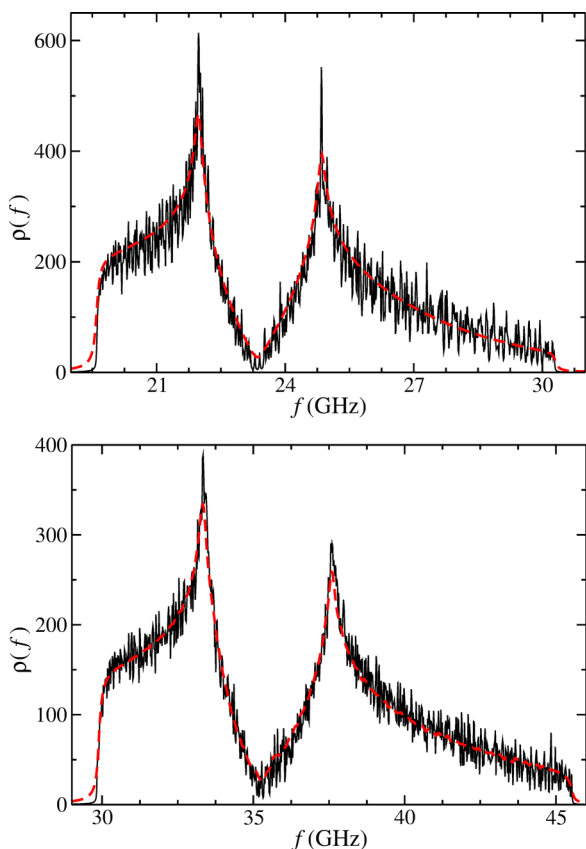
FIG. 29. (Color online) Same as Fig. 28 for the experimental DOS. The red dashed lines show the fits of the DOS deduced from the Hamiltonian in Eq. (60) to the experimental ones.

FIG. 30. (Color online) The height $\rho^{\max}$ of the van Hove peaks in the DOS of photonic crystals of varying size versus the logarithm of the number of hexagonal cells N_c. Black dots: numerical results for photonic crystals with the shape of Africa. The dashed line shows a straight-line fit $a \ln(N_c) + b$ through these data, where the resulting slope equaled $a = 0.141$. Red squares: numerical results for photonic crystals with the shape of a rectangle. Turquoise triangles: experimental results.

and for the crystal with the shape of Africa $\lambda^{(I)} = 2.198$ GHz, $\lambda^{(II)} = 0.107$ GHz, $\lambda^{(III)} = -0.013$. The data exhibit both the van Hove singularities [37] and a vanishing DOS at the Dirac frequency [9].

The DOS diverges logarithmically at the van Hove singularities only for two-dimensional, periodic structures of infinite extent. In the crystals used in the experiments, however, the sharp peaks in the DOS have a finite height $\rho^{\max}$. We determined $\rho^{\max}$ for the experimental DOS of the two microwave photonic crystals and a third, smaller one which contained only 267 cylinders, and also performed numerical studies for photonic crystals of various sizes with the shapes of a rectangle and of Africa. For a comparison of these results, we rescaled the frequencies such that the distance between the van Hove singularities was 2 for all systems. The experimental and numerical studies revealed that the maxima of the DOS, $\rho^{\max}$, behave like

$$\rho^{\max} \simeq a N_c [\ln(N_c) + b] \qquad (67)$$

with N_c denoting the number of unit cells, i.e., of hexagons formed by the voids in the photonic crystal (see Fig. 30). Here, a and b are fit parameters, where the former takes a similar value $a \sim 0.141$–$0.155 \approx \frac{3}{2\pi^2}$ for all cases, i.e., it seems to be *universal*.
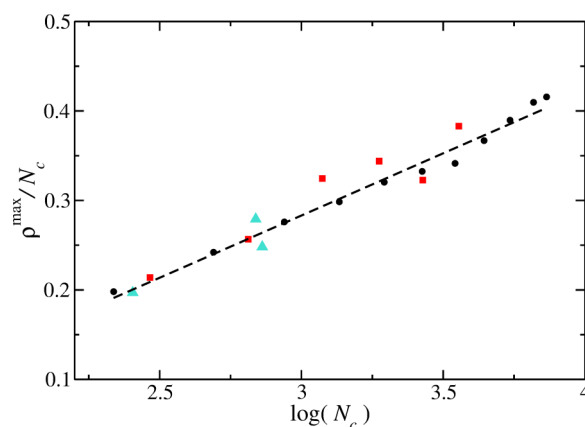
IX. CONCLUSIONS

In this paper, $1d$ (transverse out-of-plane) z vibrations have been studied. For the analysis of the experimental data, one needs to generalize the method to $2d$ (longitudinal in-plane) xy vibrations. In the algebraic approach, this is done by introducing the Lie algebra $g = u(3)$ [42,43]. The combined algebra at each site is then $u(2) \oplus u(3)$. The application of the algebraic method to longitudinal vibrations and to combinations of transverse and longitudinal vibrations will be reported in a subsequent publication. Also, for those situations in which the lattice is not composed of identical units $X - X - X - \ldots$, but it has alternating units $X - Y - X - Y - \ldots$, one needs to compute the phonon dispersion relation both for the optical and acoustic branches. This is easily done within the framework of the algebraic theory discussed here.

Finally, we have presented a method for calculating the energy spectrum (EDR) and density of states (DOS) of vibrations of solids, both harmonic and anharmonic, and applied it to the study of the EDRs and the DOSs of 1D linear chains and 2D square and hexagonal lattices. Our results have been compared with data obtained in microwave photonic crystals for 2D hexagonal lattices. These data show the expected occurrence of both van Hove singularities and Dirac zeros. The method can be easily extended to other 2D lattices, with symmetry of the unit cell other than D_{4h} and D_{6h}, and in fact to any two-dimensional structure planar and nonplanar, as for example fullerene C_{60} with icosahedral symmetry I_h. The algebraic method can also be used to calculate the response of a solid to infrared (IR) and Raman (R) radiation. For 1D systems, this response was studied in [29]. For 2D systems, it remains to be done.

The method is also well suited to study the general Hubbard boson Hamiltonian of Eq. (24). Because of the formal equivalence between the boson Hamiltonian (58) and the fermion Hamiltonian (59), it can also be used to study the

band structure in 1D, 2D square and hexagonal lattices in the tight-binding model. The DOS of the fundamental vibration $v = 1$ of a hexagonal lattice is identical to the DOS of electrons in the same lattice.

[1] K. S. Novoselov, A. K. Geim, S. V. Morozov, D. Jiang, Y. Zhang, S. V. Dubonos, I. V. Gregorieva, and A. A. Firsov, Science **306**, 666 (2004).

[2] C. W. J. Beenakker, Rev. Mod. Phys. **80**, 1337 (2008).

[3] A. H. Castro Neto, F. Guinea, N. M. R. Peres, K. S. Novoselov and A. K. Geim, Rev. Mod. Phys. **81**, 109 (2009).

[4] R. Saito, G. Dresselhaus, and M. S. Dresselhaus, *Physical Properties of Carbon Nanotubes* (Imperial College Press, London, 1998).

[5] W. Andreoni, *The Physics of Fullerene-Based and Fullerene-Related Materials* (Springer, Berlin, 2004).

[6] A. Richter, in *Emerging Applications of Number Theory*, The IMA Volumes in Mathematics and its Applications, edited by D. H. Hejhal, J. Friedman, M. C. Gutzwiller, and A. M. Odlyzko (Springer, New York, 1999), Vol. 109, p. 479.

[7] H.-J. Stöckmann, *Quantum Chaos: An Intoduction* (Cambridge University Press, Cambridge, 2000).

[8] E. Yablonovitch and T. J. Gmitter, Phys. Rev. Lett. **63**, 1950 (1989).

[9] S. Joannopoulos, J. D. Johnson, R. Meade, and J. Winn, *Photonic Crystals. Molding the Flow of Light* (Princeton University Press, Princeton, 2008).

[10] S. Bittner, B. Dietz, M. Miski-Oglu, P. Oria Iriarte, A. Richter, and F. Schäfer, Phys. Rev. B **82**, 014301 (2010).

[11] U. Kuhl, S. Barkhofen, T. Tudorovskiy, H.-J. Stöckmann, T. Hossain, L. de Forges de Parny, and F. Mortessagne, Phys. Rev. B **82**, 094308 (2010).

[12] A. Singha, M. Gibertini, B. Karmakar, S. Yuan, M. Polini, G. Vignale, M. I. Katsnelson, A. Pinczuk, L. N. Pfeiffer, K. W. West, and V. Pellegrini, Science **332**, 1176 (2011).

[13] K. K. Gomes, W. Mar, W. Ko, F. Guinea, and H. C. Manoharan, Nature (London) **483**, 306 (2012).

[14] L. Tarruell, D. Greif, T. Uehlinger, G. Jotzu, and T. Esslinger, Nature (London) **483**, 302 (2012).

[15] T. Uehlinger, G. Jotzu, M. Messer, D. Greif, W. Hofstetter, U. Bissbort, and T. Esslinger, Phys. Rev. Lett. **111**, 185307 (2013).

[16] M. Polini, F. Guinea, M. Lewenstein, H. C. Manoharan, and V. Pellegrini, Nat. Nanotechnol. **8**, 625 (2013).

[17] M. Bellec, U. Kuhl, G. Montambaux, and F. Mortessagne, Phys. Rev. Lett. **110**, 033902 (2013).

[18] M. C. Rechtsman, J. M. Zeuner, A. Tünnermann, S. Nolte, M. Segev, and A. Szameit, Nat. Photonics **7**, 153 (2013).

[19] A. B. Khanikaev, S. H. Mousavi, W.-K. Tse, M. Kargarian, A. H. MacDonald, and G. Shvets, Nat. Mater. **12**, 233 (2013).

[20] B. Dietz, T. Klaus, M. Miski-Oglu, and A. Richter, Phys. Rev. B **91**, 035411 (2015).

[21] P. R. Wallace, Phys. Rev. **71**, 622 (1947).

[22] S. Reich, J. Maultzsch, C. Thomsen, and P. Ordejón, Phys. Rev. B **66**, 035412 (2002).

[23] F. Iachello and R. D. Levine, *Algebraic Theory of Molecules* (Oxford University Press, Oxford, 1995).

[24] S. Flügge, *Practical Quantum Mechanics* (Springer, Berlin, 1974).

[25] Y. Alhassid, F. Gürsey, and F. Iachello, Ann. Phys. (NY) **148**, 346 (1983).

[26] F. Iachello and S. Oss, Phys. Rev. Lett. **66**, 2976 (1991).

[27] F. Iachello and S. Oss, Chem. Phys. Lett. **205**, 285 (1993).

[28] E. Majorana, Z. Phys. **81**, 137 (1933)

[29] F. Iachello and P. Truini, Ann. Phys. (NY) **276**, 120 (1999).

[30] T.D. Kühner and H. Monien, Phys. Rev. B **58**, R14741 (1998).

[31] W. A. Nierenberg, J. Chem. Phys. **19**, 659 (1951).

[32] F. Iachello and A. Del Sol Mesa, J. Math. Chem. **25**, 345 (1999).

[33] W. A. Bowers and H. B. Rosenstock, J. Chem. Phys. **18**, 1056 (1950).

[34] E. B. Wilson, Jr., J. C. Decius, and P. C. Cross, *Molecular Vibrations* (McGraw-Hill, New York, 1955).

[35] J. P. Hobson and W. A. Nierenberg, Phys. Rev. **89**, 662 (1953).

[36] J. Wurm, K. Richter, and İ. Adagideli, Phys. Rev. B **84**, 075468 (2011).

[37] L. Van Hove, Phys. Rev. **89**, 1189 (1953).

[38] B. Dietz and A. Richter, Chaos **25**, 097601 (2015).

[39] S. Bittner, B. Dietz, M. Miski-Oglu, and A. Richter, Phys. Rev. B **85**, 064301 (2012).

[40] B. Dietz, F. Iachello, M. Miski-Oglu, N. Pietralla, A. Richter, L. von Smekal, and J. Wambach, Phys. Rev. B **88**, 104101 (2013).

[41] M. V. Berry and R. J. Mondragon, Proc. R. Soc. London, Ser. A **412**, 53 (1987).

[42] F. Iachello and S. Oss, J. Chem. Phys. **104**, 6956 (1996).

[43] F. Iachello and F. Perez-Bernal, J. Chem. Phys. A **113**, 13273 (2009).